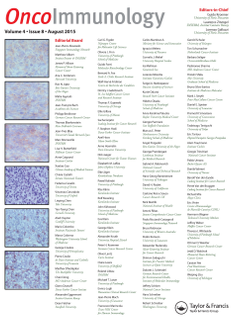

OncoImmunology

ISSN: 2162-402X (Online) Journal homepage: www.tandfonline.com/journals/koni20

Membrane IL-18 identifies a human macrophage subset with distinct proteomic and functional traits

Chiara Vitale , Andrea Petretto , Katia Cortese , Sonia Carta , Alessandra Dondero , Chiara Lavarello , Davide Cangelosi , Martina Morini , Francesca Bellora , Pietro Arnaldi , Fabrizio Loiacono , Santina Bruzzone , Francesco Piacente , Silvia Bruno , Martina Serra , Annamaria Pessino , Serafina Mammoliti , Alberto Garaventa , Massimo Conte , Massimo Locati , Giuseppe Danilo Norata , Marco Colonna , Eric Vivier , Cristina Bottino & Roberta Castriconi

To cite this article: Chiara Vitale , Andrea Petretto , Katia Cortese , Sonia Carta , Alessandra Dondero , Chiara Lavarello , Davide Cangelosi , Martina Morini , Francesca Bellora , Pietro Arnaldi , Fabrizio Loiacono , Santina Bruzzone , Francesco Piacente , Silvia Bruno , Martina Serra , Annamaria Pessino , Serafina Mammoliti , Alberto Garaventa , Massimo Conte , Massimo Locati , Giuseppe Danilo Norata , Marco Colonna , Eric Vivier , Cristina Bottino & Roberta Castriconi (2025) Membrane IL-18 identifies a human macrophage subset with distinct proteomic and functional traits, OncoImmunology, 14:1, 2571774, DOI: 10.1080/2162402X.2025.2571774

To link to this article: https://doi.org/10.1080/2162402X.2025.2571774

ONCOIMMUNOLOGY
2025, VOL. 14, NO. 1, 2571774
https://doi.org/10.1080/2162402X.2025.2571774

Taylor & Francis
Taylor & Francis Group

RESEARCH ARTICLE

OPEN ACCESS Check for updates

Membrane IL-18 identifies a human macrophage subset with distinct proteomic and functional traits

Chiara Vitale[a], Andrea Petretto[b], Katia Cortese[a], Sonia Carta[c], Alessandra Dondero[a,c], Chiara Lavarello[b], Davide Cangelosi[b], Martina Morini[b], Francesca Bellora[a], Pietro Arnaldi[a], Fabrizio Loiacono[c], Santina Bruzzone[a], Francesco Piacente[a], Silvia Bruno[a], Martina Serra[a], Annamaria Pessino[c], Serafina Mammoliti[c], Alberto Garaventa[b], Massimo Conte[b], Massimo Locati[d,e], Giuseppe Danilo Norata[f,g], Marco Colonna[h], Eric Vivier[i,j,k], Cristina Bottino[a,b] and Roberta Castriconi[a,b]

[a]DIMES, Department of Experimental Medicine, Università di Genova, Genova, Italy; [b]IRCCS Istituto Giannina Gaslini, Genova, Italy; [c]IRCCS Ospedale Policlinico San Martino, Genova, Italy; [d]Department of Medical Biotechnologies and Translational Medicine, Università degli Studi di Milano, Milan, Italy; [e]Humanitas Clinical and Research Center – IRCCS, Rozzano (MI), Italy; [f]Department of Pharmacological and Biomolecular Sciences, Università degli Studi di Milano, Milan, Italy; [g]Center for the Study of Atherosclerosis, E. Bassini Hospital, Cinisello Balsamo, Italy; [h]Hope Center for Neurological Disorders, Washington University School of Medicine, St. Louis, MO, USA; Brain Immunology and Glia (BIG) Center, Washington University School of Medicine, St. Louis, MO, USA; Department of Pathology and Immunology, Washington University in St. Louis School of Medicine, St. Louis, MO, USA; [i]Innate Pharma Research Laboratories, Innate Pharma, Marseille, France; [j]Aix Marseille Université, Centre National de la Recherche Scientifique, INSERM, Centre d'Immunologie de Marseille-Luminy, Marseille, France; [k]Assistance Publique-Hôpitaux de Marseille, Hôpital de la Timone, Marseille Immunopôle, Marseille, France

ABSTRACT

This study contributes to the characterization of human macrophages in normal and pathological conditions such as cancer. We characterized a macrophage population expressing membrane-associated IL-18 (mIL-18) that shows peculiar proteomic, phenotypic, ultrastructural, and functional properties. mIL-18+ macrophages exhibit increased levels of key proteins involved in pathogen recognition, activation, migration, and endocytosis. They also display specialized functions in vesicle and actin filament transport and lipid metabolism, and have typical mitochondrial traits. Importantly, mIL-18+ cells dominate the peritoneal fluid of adult cancer patients and are present in the bone marrow of children with neuroblastoma. They express high levels of TREM2 but display heterogeneous FOLR2 expression, distinguishing distinct cell subsets with possibly different functions. Accordingly, in primary neuroblastomas, transcriptional signatures associated with mIL-18 expression show different prognostic values. Our data show that mIL-18+ macrophages, which are predominant across the tumor microenvironment, exhibit previously undetected heterogeneity, potentially impacting tumor progression in a variable manner.

ARTICLE HISTORY
Received 12 March 2025
Revised 24 September 2025
Accepted 29 September 2025

KEYWORDS
Macrophages; IL-18; endocytosis; TREM2; FOLR2; adult cancer patients; pediatric neuroblastoma; proteomic-analysis

CONTACT Cristina Bottino cristina.bottino@unige.it DIMES, Department of Experimental Medicine, Università di Genova, Via Balbi 5 Genova, Italy and IRCCS Istituto Giannina Gaslini, Via Gerolamo Gaslini 5, 16147 Genova, Italy

Supplemental data for this article can be accessed online at https://doi.org/10.1080/2162402X.2025.2571774.

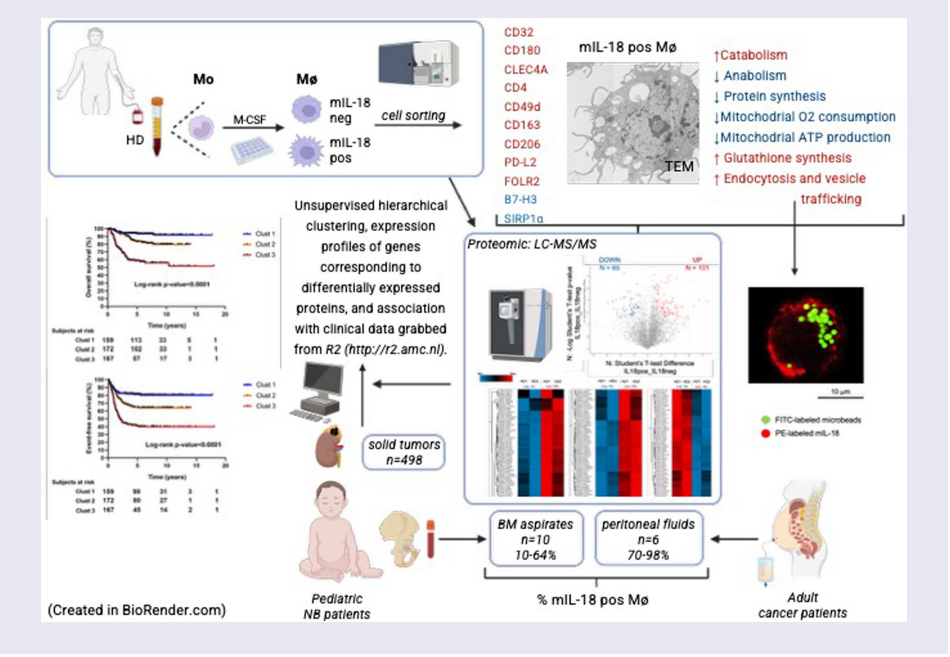

Introduction

Immunotherapy significantly impacts cancer patients' survival. However, a relevant percentage of patients show primary or acquired resistance to therapy, forcing the exploration of strategies for overcoming failures.[1-3] To understand what impacts the therapy's effectiveness, different aspects of tumors and the tumor microenvironment (TME) are being analyzed, including the "immunoscore", e.g., the number and quality of tumor-infiltrating immune cells[4-7]; these include macrophages [8] and natural killer (NK) cells [9] that communicate with each other.[10-12] The frequency and main properties of immune effectors can predict the response to immunotherapies.[8,9,11,13]

Macrophages are highly enriched in the TME. M1 and M2 indicate macrophages lying at the opposite ends of the functional polarization process, i.e., proinflammatory-tumor suppressive or reparative-tumor promoting, respectively. This simplistic dichotomy is overcome by a more updated view of macrophage polarization.[8,9,11,13,14] In vitro, M2 subpopulations can include M2a, obtained by IL-13 and IL-4 stimulation, which secrete immunomodulatory factors such as TGF-β and dampen the NK cell function. Immunosuppressive activity has also been attributed to IL-10 secretion by M2c macrophages, which differentiate in vitro upon stimulation with glucocorticoids, TGF-β, or IL-10 itself. Furthermore, the in vivo scenario could not exactly mirror what was observed in vitro, which is characterized by a complex microenvironment and cell plasticity. In vivo, tumor-associated macrophages (TAMs) can express both M1 and M2 markers, change their phenotypic/functional properties, and increase their heterogeneity over time due to microenvironment perturbations, which are also related to therapeutic agents.[11,15] In breast cancer, single-cell analysis showed the presence of seven different macrophage clusters expressing PD-L1; their relative abundance differed in estrogen receptor (ER)-positive or ER-negative tumors and tumors with different grades.[16] Recently, two distinct macrophage populations expressing TREM2 or FOLR2 have been described in breast cancer and in many other tumor types, which appear to exert opposite functions.[17] TREM2 characterizes macrophages with immunosuppressive functions; its blockade enhances CD8+ T and NK cell responses, delays tumor growth, and synergizes with immune checkpoint inhibitors.[12,18,19] In contrast, FOLR2+ macrophages are tissue-resident macrophages colonizing healthy tissues, which in tumors interact with tumor-infiltrating CD8+ T promoting their expansion and activation.

Correlating various macrophage signatures with disease tumor stages, resistance/response to therapies, and possibly planning strategies targeting the macrophage populations more significantly associated with a worse prognosis. The macrophage heterogeneity also relies on their origin since they can derive from the recruitment of circulating monocytes or precursors colonizing tissue during embryonic/fetal

development.[11,20-23] In this context, a murine model of pancreatic ductal adenocarcinoma showed that TAMs originating from fetal precursors support tumors, while bone marrow (BM)-derived macrophages have marked antigen presentation properties.[24] In both mice and humans, CX3CR1, CXCR4, CD49d, CD11b, and CD11a have been described as markers distinguishing these two cell types.[11,16,24-26] We previously contributed to dissecting the phenotypic and functional heterogeneity of TAMs by identifying a membrane form of IL-18 (mIL-18), which is expressed by a high percentage of macrophages in the peritoneal fluid of ovarian cancer patients.[27] In healthy donors, our data show that mIL-18 was expressed in 20%–40% of unpolarized macrophages (termed M0) differentiated in vitro from both non-classical CD16+ and classical CD16- monocytes in the presence of M-CSF. In contrast, GM-CSF-treated monocytes and monocyte-derived immature or mature dendritic cells lack mIL-18 expression.[28,29] IL-18 is a cytokine belonging to the IL-1 family that profoundly modulates the function of immune effectors such as NK cells.[30] To date, the precise mechanisms responsible for mIL-18 retention at the macrophage cell membrane and its release as soluble cytokines (sIL-18) are only partially characterized. mIL-18 requires caspase-1 processing, suggesting the requirement for surface expression of the pro-IL-18 to mature IL-18 conversion.[28] The acidic treatment does not modify the mIL-18 expression, suggesting that the cytokine firmly binds to the plasma membrane. mIL-18 expression is maintained upon M2 polarization, whereas it is lost upon M1 polarization of both M0 and M2 macrophages through pathogen-derived products (LPS and BCG), a process paralleled by the release of sIL-18 in the extracellular microenvironment. TLR-mediated stimuli are known to activate a broad spectrum of cellular proteases, suggesting their involvement in the release of mIL-18 as a soluble form. These proteases, however, do not include calpain, a membrane-bound cysteine protease involved in the conversion of pro-IL-1α to IL-1α; indeed, treatment with the calpain inhibitor does not affect the IL-18 release while affecting that of IL-1α.

In this study, we compared mIL-18+ and mIL-18- populations by performing proteomic analyses and analyzing their immunophenotypic, metabolic, morphologic, and ultrastructural characteristics. Additionally, we also investigated the presence of mIL-18+ myeloid populations in specimens from adult cancer patients and children with neuroblastoma (NB). Our findings expand the understanding of human myeloid and macrophage heterogeneity, revealing distinct features that may influence cancer progression and responses to immunotherapy.

Materials and methods

In vitro differentiation of M0 macrophage

Peripheral blood mononuclear cells (PBMCs) were isolated from healthy blood donor volunteers admitted to the blood transfusion center of the IRCCS Ospedale Policlinico S. Martino after obtaining written informed consent. The study was approved by the Ligurian Ethics Committee (Comitato etico territoriale, CET, Liguria) (DB id 10125). After the standard Ficoll-Paque density gradient (Euroclone S.P.A., Italy), monocytes were purified from PBMC using the Human Monocyte Cell Isolation Kit II (Miltenyi Biotec). The cells were cultured (5×10^5/mL) for 7 days in lumox plates (24 lumox multiwell TC-QUALITAET plates, Greiner bio-one GmbH, Frickenhausen, Germany) with 100 ng/mL of rM-CSF (Pepro-Tech, London, UK) to obtain M0 macrophages.[29]

Cell sorting and proteomic analysis

We isolated mIL-18+ and mIL-18- macrophages using FACS sorting with a FACSAria II instrument under low-pressure conditions, 100 mm drops, and a 4-way purity mask. Before the experiments, we validated the instrument settings using the CS&T system BD.[28] During sorting, the cell concentration was approximately 5–10 million cells/mL. The cells were then collected in complete RPMI culture medium.

The mIL-18+ and mIL-18- macrophages were analyzed using high-resolution liquid chromatography coupled with tandem mass spectrometry (LC–MS/MS) based on Orbitrap technology. Protein quantification was carried out using a label-free approach (LFQ) within the MaxQuant suite.[30,31] Statistical validation of the data was performed using tools from Perseus Software.[31,32]

Gene ontology (GO) enrichment analysis was conducted using the ShinyGO web server (version 0.76.1), which uses an extensive annotation database derived from Ensembl and STRING-db.[33] The functional networks of the proteins in various pathways were identified using Enrichr-KG, a knowledge graph database and web server application that integrates selected gene set libraries from Enrichr DB for enrichment analysis and visualization. The libraries used for this analysis were Reactome 2022, KEGG 2021Human, GO Biological Process 2021, and WikiPathway 2021 Human. The enrichment results were presented as subgraphs with nodes and links connecting genes to their enriched terms. Enrichr-KG also allows the addition of gene-gene links and predicted genes to these subgraphs.[34]

For the proteomic analysis, macrophages were processed using the iST protocol. The pellets were solubilized with 25 µL of 6 M GdmCl, 10 mM TCEP, 40 mM CAA, and 100 mM Tris pH 8.5, then lysed, reduced, and alkylated by three cycles of heat and thaw, followed by 30 min of sonication. The samples were loaded onto a StageTip with a 1 SDB-RPS disk. The lysates were diluted with 10% (v/v) ACN and 25 mM Tris pH 8.5, then digested overnight at 37 °C with 0.5 µg of Lys-C and 0.5 µg of trypsin. After digestion, the samples were acidified with 100 µL of 1% (v/v) TFA and washed three times with 0.2% (v/v) TFA. Elution was performed with 60 µL of 5% (v/v) ammonium hydroxide and 80% (v/v) CAN.[30] Peptide separation was conducted using the Dionex Ultimate 3000 RSLC nanoSystem. The samples were loaded from the sample loop onto a trapping column (2 cm × 100 µm ID, Acclaim PepMap C18, 2 µm particles, 100 Å pore size; Thermo Scientific) using a loading solvent of 98% H_2O and 2% CH_3CN with 0.1% formic acid at a flow rate of 5 µL/min for 5 min. The trapping column was then switched in line with the separation column, and the peptides were eluted with an increasing gradient of organic solvent at a flow rate of 300 nL/min. Peptides were separated on an EASY-Spray column (25 cm × 75 µm ID, PepMap C18, 2 µm particles, 100 Å pore size; Thermo Scientific) thermostated at 60 °C. A multi-step gradient of 5%–30% solution B (80% CH_3CN and 20% H_2O with 0.1% formic acid) was applied over 170 min, followed by a 30%–45% solution B gradient for 35 min.[30]

The mass spectrometer, LTQ-Orbitrap Velos Pro, was operated in positive ionization mode. MS survey scans were performed in the Orbitrap over a mass range of 375–1500 m/z with a resolution of 100,000.[30] The automatic gain control was set at 1,000,000, with a maximum ion injection time of 250 ms. Data were collected in a data-dependent acquisition mode with alternating MS and MS/MS experiments. The minimum MS signal required to trigger MS/MS was set to 10,000 ions, with the most intense signal selected for MS/MS using a 2 Da isolation window. Ions already selected for MS/MS were excluded for 25 s, with an exclusion window size of ± 10 ppm. A single micro-scan was recorded for each MS scan, and CID was performed in the linear ion trap with a target value of 3,000 ions, a maximum ion injection time of 50 ms, a normalized collision energy of 35%, a *Q*-value of 0.25, and an activation time of 10 ms. A maximum of 10 MS/MS experiments were triggered per MS scan.[30]

The raw data from the mass spectrometry experiments were analyzed using MaxQuant software (version 1.6.1.0). The protein and peptide false discovery rates FDR were set at 0.01, and the peptides had to be at least 6 amino acids long. A time-dependent mass recalibration algorithm was employed to increase the mass accuracy of the precursor ions. MS/MS spectra were searched using the Andromeda search engine integrated into MaxQuant against the UniProt Human database, combined with 248 common contaminants and reversed sequences. Trypsin was selected for enzyme specificity.[30] Cysteine carbamidomethylation was set as a fixed modification, while protein *N*-terminal acetylation, methionine oxidation, and deamidation (*N*, Q) were allowed as variable modifications. A maximum of two missed cleavages was permitted. The initial precursor mass deviation reached 7 ppm, and the fragment ion deviation was set to 0.5 Da. Quantification was performed using MaxLFQ with the "Match between runs" option (time window of 1 min).[30]

mAbs

Anti-human IL-18 mAb (mouse IgG1, clone 125-2H) and anti-CX3CR1-PE (rat IgG2b, clone 2A9-1) were purchased from Medical and Biological Laboratories; anti-CD14-VioBlue (recombinant human IgG1, clone REA599), anti-CD68-PEVIO770 (recombinant human IgG1, clone REA886), anti-FcgRIIA (CD32)-APC (mouse IgG2a, clone 2E1), anti-SIRP1α (CD172a)-APC (recombinant human IgG1, clone REA144), anti-CD4-APC (recombinant human IgG1, clone REA623), anti-B7H3 (CD276)-APC (mouse IgG2b,

clone FM276), anti-ITGA4 (CD49d)-APC (recombinant human IgG1, clone REA545), anti-CD180-APC (recombinant human IgG1, clone REA956), anti-HLA-DR-APC (recombinant human IgG1, clone REA805), anti-CLEC4A (CD367)-APC (recombinant human IgG1, clone REA329) were purchased from Miltenyi Biotec; anti-CD45-APC-H7 (mouse IgG1, clone 2D1), anti-CD163 (mouse IgG1, clone GHI/61), anti-CD206-FITC (mouse IgG1, clone 19.2), anti-CD80-PE (mouse IgG1, clone B7-1) were purchased from BD Biosciences (San Diego, CA); anti-PD-L1.3.1 (IgG1) and anti-PD-L2 (IgG1) mAbs were produced in D. Olive's laboratory; anti-CXCR4 (mouse IgG2b, clone 12G5) and anti-CCR2 (mouse IgG2b) were purchased from R&D Systems (Minneapolis, MN); anti-TREM2-APC (Rat IgG2b, clone 237920) and Rat IgG2b isotype control were purchased from bio-techne; anti-FOLR2-PE (mouse IgG1, clone EM-35) and mouse IgG1 isotype control were purchased from ThermoFisher Scientific; MA127 (mouse IgG1, anti-NTBA) mAb was produced in our lab.

VioBlue, PEVIO770, APC, FITC, APC-H7, PE isotype-matched mouse (Miltenyi Biotec or BD Biosciences) or rat (Medical and Biological Laboratories) mAbs were used as negative controls.

Immunofluorescence and flow cytometry

For one-color flow cytometry analysis (FACSCalibur, Becton Dickinson & Co., Mountain View, CA), cells were stained with the appropriate monoclonal antibodies (mAbs) for 30 min at 4 °C, washed once with BD FACSflow containing 5% FCS, and then stained with Phycoerythrin (PE)-conjugated isotype-specific goat anti-mouse secondary reagent (Southern Biotechnology Associates, Birmingham, AL) for 30 min at 4 °C. During each experimental session, the performance of the flow cytometer was checked, and the reproducibility of the fluorescence intensity was verified using calibrated microspheres (Becton Dickinson & Co., Mountain View, CA). Isotype-matched PE-conjugated goat anti-mouse secondary reagent was used as a control.[35]

For multiparametric flow cytometry (MFC) analysis, all samples were first incubated for 10 min with human Fc receptor Blocking Reagent (Miltenyi Biotec, Bergisch Gladbach, Germany), washed once with serum-free RPMI 1640 medium, and then incubated with both fluorochrome-conjugated primary antibodies and Fixable Viability Stain 510 (BD) to exclude dead cells (15 min at room temperature). Finally, the samples were resuspended in 500 µL of FACSflow (5% FCS) before acquisition using the FACSVerse flow cytometer (BD). BD FACSuite CS&T Beads were used daily to monitor cytometer performance.

For analysis of one-color flow cytometry data, CellQuestPro software was used, while FACS Suite software (Becton Dickinson, Mountain View, CA) was employed for analyzing MFC acquisition files.[35]

Transmission electron microscopy (TEM)

Sorted mIL-18+ and mIL-18- human macrophages were washed out twice in cacodylate buffer (0.1 M Sigma–Aldrich, St. Louis, MI, USA) and fixed for 1 h at room temperature using a 2.5% v/v glutaraldehyde solution (Electron Microscopy Science, Hatfield, PA, USA) diluted in 0.1 M cacodylate buffer. The cells were postfixed in 1% w/v osmium tetroxide for 10' (VWR International, PA, USA) and 1% w/v aqueous uranyl acetate (SERVA Electrophoresis GmbH, Heidelberg Germany) for 1 h. The samples were subsequently dehydrated through a graded ethanol series (Merck, Darmstadt, Germany) and embedded in epoxy resin (Poly-Bed; Polysciences, Inc., Warrington, PA) for 48 h at 60 °C. Ultrathin sections (50 nm) were cut and counterstained with 5% w/v uranyl acetate in 50% v/v ethanol. Electron micrographs were acquired as single snapshot and/or multiple image alignment (MIA) using a Hitachi 7800 120 Kv electron microscope (Hitachi, Tokyo, Japan) equipped with a Megaview G3 digital camera and Radius software (EMSIS, Muenster, Germany). To perform human macrophage size analysis, the diameter of 25 whole cells was measured with the line tool embedded in Radius 2.0 software. To perform mitochondria morphometry, 35 whole cells were scored for mitochondria and measured with the line and area tools of Radius 2.0 software. For rough endoplasmic reticulum (RER) morphometry, 25 whole cells were scored for rER, and each cisterna was measured at three different points. The results were plotted as histograms with data points (mean ± SD). Statistical analyses were performed using GraphPad Prism. A Mann–Whitney U test was performed to evaluate the cell size and mitochondria diameter, while a *t*-test was performed to

evaluate mitochondria density and ER size. Mean differences were considered statistically significant at $p < 0.05$.

Metabolic activity

The oxygen consumption rate (OCR) and extracellular acidification rate (ECAR) were determined using a Seahorse XFp (Agilent Technologies). Briefly, 80,000 mIL-18+ or mIL-18- sorted macrophages were seeded in XFp cell plates. The OCR and ECAR were determined using the Seahorse XFp Extracellular Flux Analyzer (Agilent Technologies, Santa Clara, CA, USA). The cells were incubated at 37 °C for 45' in a no-CO2 incubator with Agilent Seahorse DMEM, pH 7.4, enriched with glucose (11 mM), glutamine (2 mM), and pyruvate (1 mM). The bioenergetic profile was measured using the Cell Mito Stress Test Kit and a real-time ATP rate assay according to the manufacturer's instructions. Three measurements of the OCR and ECAR were taken under control conditions and after sequential injections of 1.5 μM oligomycin, 1.5 μM FCCP, and 0.5 μM rotenone plus 0.5 μM antimycin A (cell mito stress test) or after sequential injection of 1.5 μM of oligomycin and 0.5 μM each of rotenone/antimycin A (ATP rate assay).

Endocytosis

The endocytic properties of mIL-18+ and mIL-18- macrophages were evaluated by using fluorescent yellow–green carboxylate latex beads (Sigma–Aldrich). Briefly, 500.000 cells were incubated for 30' at 37 °C with a bead suspension at a final dilution of 4 μL/ml. The cells were then washed twice in a complete RPMI medium and analyzed by MFC, analyzing mIL-18, CD68, CD163, and NTBA (CD352) molecules on three different cell gates characterized by null (Gate 1), low (Gate 2), or high (Gate 3) beads-associated fluorescence.

Confocal microscope analysis

Confocal microscopic analysis was performed as previously described.[36] The macrophages were layered on a 0.17 mm-thick microscope coverslip (optically clear borosilicate glass) and examined on the laser scanning confocal microscope SP2-AOBS (Leica Microsystems, Mannheim, Germany), using either a HC PL APO 20x/0.70 objective or a HCX PL APO 40 × /0.75–1.25 oil immersion objective on a DM IRE2 inverted microscope. Fluorescent dye excitation was performed using the 488 nm line of the Argon laser for excitation of the fluorescent latex beads (emission detection range 500–535 nm), and the 546 nm line of the He/Ne laser for excitation of phycoerythrin-conjugated mIL-18 (emission detection range 555–650 nm). Leica software was used for image acquisition (1024 × 1024 × 8 bit), while analysis was performed with Leica software or ImageJ.

Patient's samples

Supplemental Table 4 summarizes the clinical data of adult and pediatric cancer patients whose samples were analyzed in this study. Age and sex were included.

The peritoneal fluids were collected from anonymized adult cancer patients admitted at the Medical Oncology Unit and Department of Internal Medicine, IRCCS S. Martino-IST and University of Genova, Genova, Italy. All the biological samples were collected after obtaining written informed consent, and the study was approved by the Ligurian Ethical Committee (CET Liguria) (DB id 12889). Patients were eligible if they had measurable disease at first presentation or after relapse and were treatment naive.

BM aspirates derived from pediatric NB patients enrolled at IRCCS Istituto G. Gaslini. All the samples were collected by Biobanca Integrata Tessuto-genomica – BIT, Istituto IRCCS G. Gaslini, Genova, Italy, after written informed consent by the parents or legal guardians. The histological diagnosis was made on tumor samples (surgical or core biopsies or surgical specimens from resection) paired with BM aspirates analyzed in this study. The staging was established according to the International Neuroblastoma Staging System[37,38] with NB infiltration evaluated by cytomorphological analysis. The investigation was performed

after approval by the Ligurian ethical committee (CET Liguria) (number 004-28/05/2018). The committee and the procedures followed the Helsinki Declaration of 1975.

Prognostic value of the mRNA signature codifying for the proteins up- and down-regulated in mIL-18+ M0 macrophages

The differential gene expression (DEG) between mIL-18+ and mIL-18- macrophage samples was visualized by heat map using Morpheus, a versatile matrix visualization and analysis software (https://software.broadinstitute.org/morpheus). Unsupervised hierarchical clustering was used to segregate patients and genes into distinct homogenous groups. Only the top clusters from the dendrograms were selected for further evaluation. Clustering analysis of genes was performed by grouping clusters to maintain the separation between up- and down-regulated genes. To this end, the "Group columns by" option was selected in the web interface. Heat map visualization and unsupervised clustering analysis were performed on publicly available gene expression profiles of primary tumors collected at diagnosis from 498 NB patients. Gene expression profiles and associated clinical data were grabbed from R2: Genomics Analysis and Visualization Platform (http://r2.amc.nl). The expression levels were adjusted with the robust z-score transformation option that was available on the web platform. The chi-square test was used to assess the significance of the association between clusters and selected patients' characteristics. *P*-values lower than 0.001 were considered statistically significantly associated.

The two main endpoints of the prognostic analysis were the overall survival (OS) and the event-free survival (EFS). OS and EFS curves were plotted by the Kaplan–Meier method and were compared with the log-rank test. *P*-values lower than 0.005 were considered significant. GraphPad Prism version 8.0 for Microsoft Windows, www.graphpad.com, was used to plot Kaplan–Meier curves and to compute log-rank *p*-values.

Statistical analysis

The non-parametric significance test, Wilcoxon–Mann–Whitney *p*-value, was used to verify whether two independent samples of observations have equally large values. The test is a statistical tool suitable for analyzing the rank sum of two independent groups. (*p*) indicates the statistical level of significance.

A *t*-test was employed with the assumption of a normal distribution of data in the measurements (two unpaired groups; two tails). Graphic representation and statistical analyses were performed using the PASW Statistic version 20.0 software and GraphPad Prism 6.

Generative AI

Some authors have used ChatGPT (GPT-4, provided by OpenAI) to increase the readability of certain sections of this manuscript. After utilizing this tool, the authors thoroughly reviewed and edited the content as needed and have full responsibility for the final content.

Results

Proteomic analysis of mIL-18+ and mIL-18- human macrophages reveals significantly different molecular signatures

Classical CD68+ unpolarized M0 macrophages were obtained by culturing, and in the presence of M-CSF, monocytes were isolated from the peripheral blood mononuclear cells PBMC of two unrelated healthy donors (HD1 and HD2). According to previous data,[28,29] a membrane-bound form of IL-18 (mIL-18) was expressed at the cell surface of an M0 subset; this represented 45% and 61% of the macrophages derived from HD1 and HD2, respectively. The mIL-18+ and mIL-18- subsets were sorted, and their purity was confirmed by immunofluorescence and flow cytometry (IF–FC) (Figure 1A).

The sorted M0 subsets were analyzed by high-resolution mass spectrometry. Data processing through the MaxQuant software allowed the identification of a total of 4637 proteins, of which 3833 were quantified using a label-free quantitation approach. The unsupervised PCA analysis of the whole protein

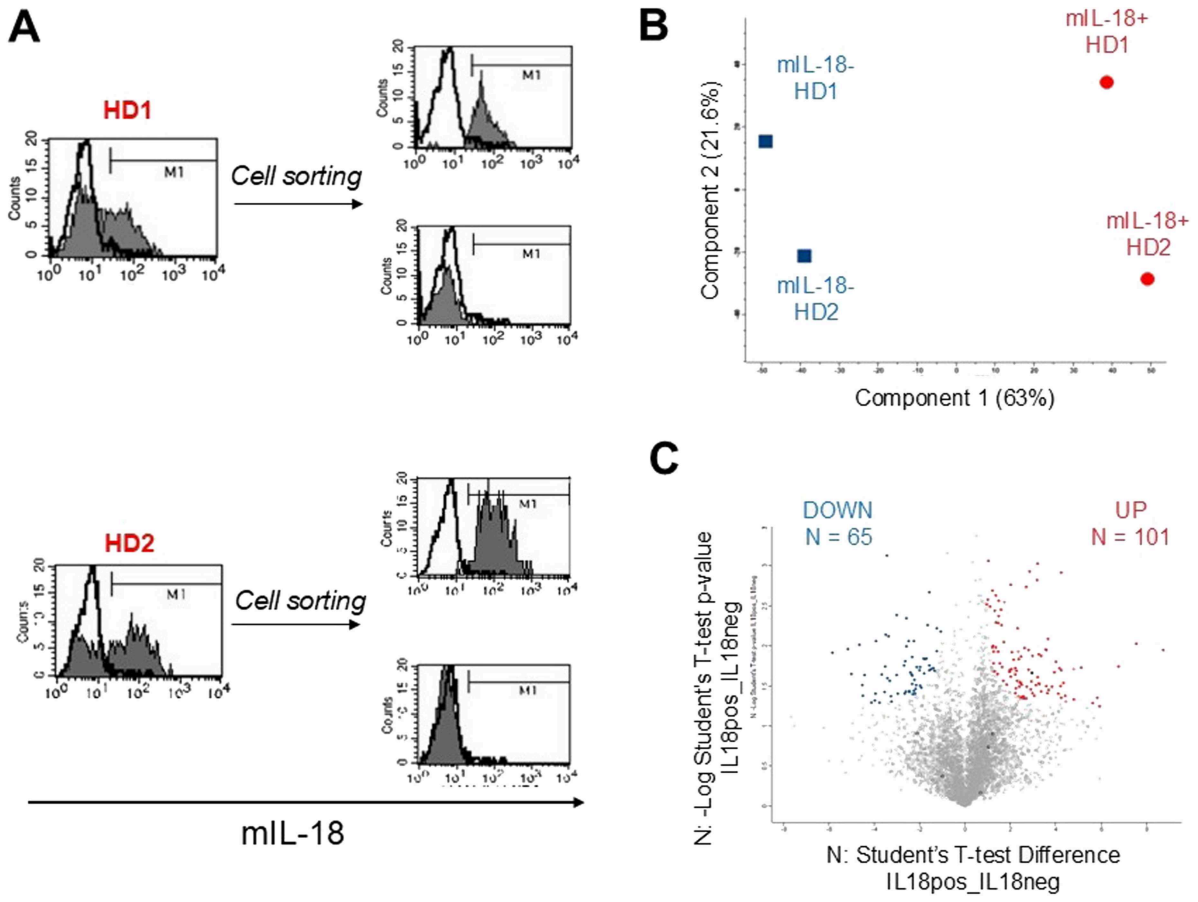

Figure 1. Proteomic analysis of mIL-18+ and mIL-18- macrophages. (A) Macrophages from two healthy donors (HD1 and HD2) were analyzed by IF–FC for mIL-18 expression before and after cell sorting. (B) Unsupervised PCA analysis. (C) Volcano plot representation of proteins differentially expressed in mIL-18+ vs mIL-18- macrophages. The colored dots represent proteins displaying both large magnitude fold-changes (*x*-axis) and high statistical significance (FDR = 0.05 and s0 = 0.1 log10 of *P*-value, *y*-axis) between the two populations.

content of our dataset indicated that the mIL-18+ and mIL-18- subsets accounted for more than 60% of the variation in their phenotype (Component 1) and were separated into different clusters (Figure 1B). As shown by the volcano plot, the protein quantification revealed a set of 166 differentially expressed proteins, of which 65 proteins were down-regulated and 101 up-regulated in mIL-18+ as compared to mIL-18- cells (Figure 1C). The protein expression profile of mIL-18+ and mIL-18- macrophages and the identity of the differentially expressed proteins are shown in the unsupervised hierarchical clustering analysis (Figure 2).

Using IF–FC, we validated the proteomic data, analyzing the surface expression of selected plasma membrane-associated proteins that emerged upregulated in mIL-18+ cells (Figure 3, panels A–C). The analysis confirmed increased expression of CD32 (FcγRIIA), CD180, CLEC4A, CD4, CD49d (ITGA4), and CD163 in mIL-18+ macrophages. We also included surface molecules that did not emerged from the proteomic analysis but are relevant to macrophage biology. mIL-18+ cells expressed higher levels of CD206 and PD-L2, and, conversely, significantly lower levels of B7-H3 and SIRP1α. HLA-II and PD-L1 were expressed at similar levels in the two macrophage populations.

M0 unpolarized macrophages derived from three additional HDs were analyzed for TREM2 and FOLR2 expression, two markers identifying distinct macrophage populations in tumor or healthy tissues.[17] As shown in Figure 3, panels D and E, TREM2 was weakly expressed by all the macrophages. On the other hand, two mIL18+ subsets, one expressing FOLR2 and the other lacking it, were identified. mIL-18+ cells expressed a significantly greater amounts of FOLR2 compared to mIL-18- cells. An opposite expression trend was observed for SIRP1α, which was analyzed as a control. Indeed, mIL-18+ cells expressed significantly lower levels of SIRP1α compared to mIL-18- cells.

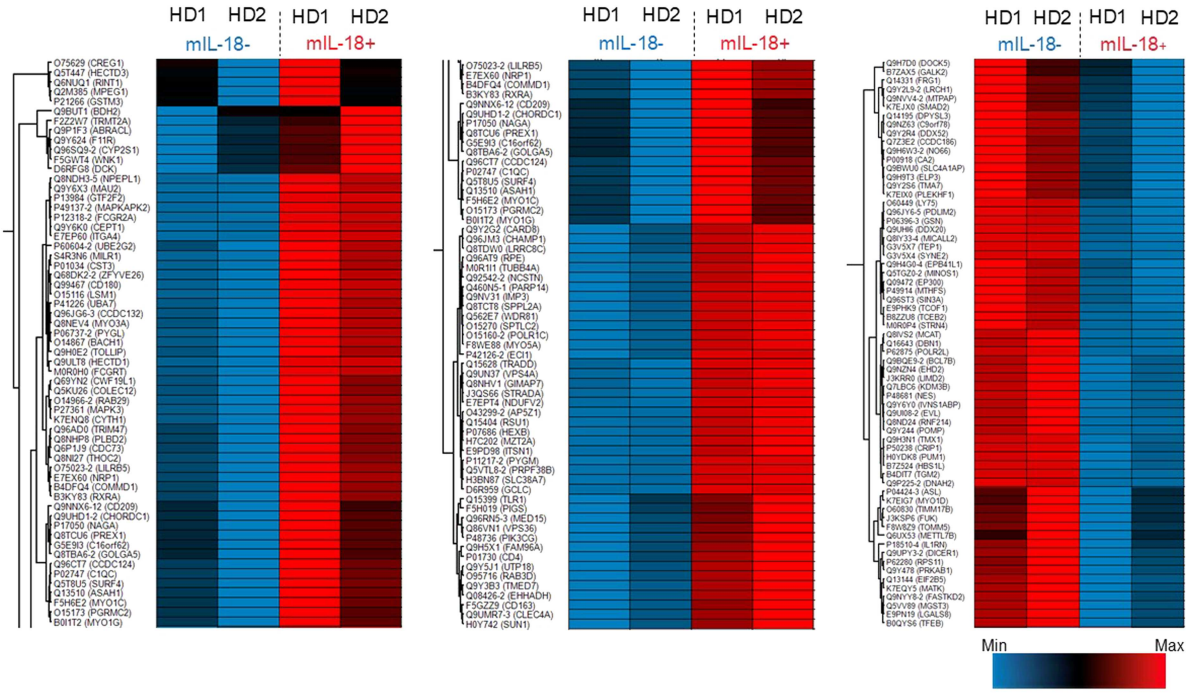

Figure 2. Unsupervised hierarchical clustering analysis. The graphics show the unsupervised hierarchical clustering analysis of significant proteins (out of the 3833 quantified proteins), differentially expressed in paired mIL-18+ and mIL-18- macrophages *t*-tests from HD1 and HD2. Protein expression levels were z-scored and log2 transformed and are indicated by a two-color scale ranging from blue (lowest values) to red (highest values), reported in the horizontal bar at the top of the figure. Each column corresponds to a sample (indicated on the top side), and each row represents a differentially expressed protein.

Proteomics highlighted important differences in the molecular repertoire of mIL-18+ and mIL-18- macrophages. Notably, however, as indicated by IF–FC analysis, proteomics may even underestimate the surface protein profile owing to the still limited sensitivity of mass spectrometry and its differing ability to identify and quantify surface versus soluble proteins.

mIL-18+ macrophages show enrichment in proteins involved in endocytosis, lipidic catabolism, pathogen recognition, activation and migration

To associate the proteins that emerged from the proteomic analysis with specific molecular and functional pathways, we conducted a gene ontology (GO) enrichment analysis using the ShinyGO web server. As shown in Supplemental Figure 1 and Supplemental Table 1, mIL-18+ cells showed upregulation of proteins involved in the generation of cell protrusions (axonogenesis) (NRP1, ITGA4), vesicle transport (MYO1G, MYO5A, MYO1C) and lipidic catabolic processes, including the degradation of ceramide and fatty acid membrane lipids (HEXB, ASAH1, PIK3CG, EHHADH, PLBD2, PDH2, ECI1, NAGA). Proteins upregulated in mIL-18+ macrophages also included several molecules involved in leukocyte pathogen recognition, activation, and migration (HEXB, TOLLIP, HECTD1, PYGL, CST3, ASAH1, RAB3D, PIK3CG, ITGA4, RAB29, PREX1, CD180, CREG1, NCSTN, MILR1, SURF4). The leukocyte pathways were also characterized by the upregulation of CD4, CD209, CLEC4A, FCGR2A, and TLR1 (Supplemental Table 1).

To expand the panorama of the functional pathways upregulated in mIL-18+ cells, we explored different gene set libraries combined with the use of the web-server application Enrichr-KG[34] (Supplemental Figure 2, left panel and Supplemental Table 2). This analysis also provided a subnetwork linking the most highly enriched terms with proteins upregulated in different libraries (Supplemental Figure 2, Right Panel). mIL-18+ cells showed a protein repertoire highly involved in innate immune responses against pathogens such as pathogenic *Escherichia coli*, *Mycobacterium tuberculosis*, and Yersinia (TRADD, TLR1, MAPK3, CD209, FCGR2A, VPS36, CD4, SURF4), cell activation and degranulation (TOLLIP,

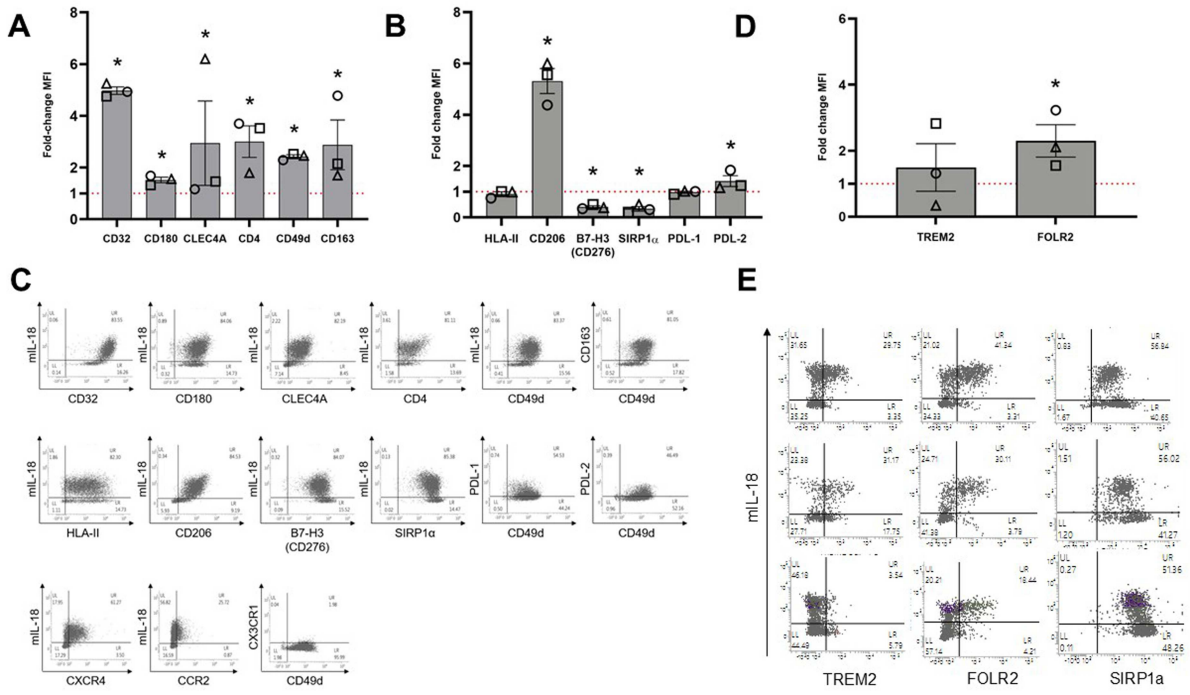

Figure 3. Surface phenotyping of mIL-18+ and mIL-18- macrophages. (A, B) M0 macrophages from three healthy donors were analyzed by IF–FC for the expression of the indicated molecules, gating on mIL-18+ or mIL-18- cells. (C) Representative double IF–FC of the expression of mIL-18 and the indicated surface markers in M0 macrophages. Owing to mAbs availability and compatibility with the isotype of the anti-mIL-18 mAb, some molecules were analyzed compared to molecules highly co-expressed with mIL-18, such as CD49d. (D, E) Statistical and representative analysis (IF–FC) of the expression of mIL-18, TREM2, FOLR2, and SIRP1α (control) in M0 macrophages from three healthy donors. In panels A, B, and D, the value = 1 was arbitrarily assigned to the level of protein expression (MFI) in mIL-18- cells. The symbols represent values from different donors. The graphs display the mean ± SEM of the MFI fold changes. The difference between groups was analyzed by one-way ANOVA with the Bonferroni post-test by GraphPad Prism. * = $p < 0.05$.

RAB3D, FCGR2A). Moreover, the analysis confirmed in mIL-18+ cells the upregulation of proteins activated upon TLR or IL-1R engagement (PIK3CG, TMED7, TLR1, MAPK3, TOLLIP, CD180), involved in fatty acid oxidation (mitochondrial ECI1 and EHHADH), and crucial for ceramide catabolism (NAGA, HEXB, ASAH1). The latter lipidic catabolic pathway causes sphingosine production; in line with this, the sphingolipid signaling pathway was upregulated (TRADD, ASAH1, SPTLC2, MAPK3). Importantly, these data also showed an increased vesicle-mediated and actin filament-based transport in mIL-18+ cells (MYO5A, MYO1C, MYO1G, CD163, VPS4A, VPS36, ITSN, TMED7, and COLEC12) (Supplemental Figure 2). Interestingly, mIL-18+ also had a reduced expression of SMAD2, a key protein involved in the signal transduction of TGF-β.[39]

The analysis of the biological processes associated with the 65 proteins downregulated in mIL-18+ macrophages suggested a restriction of pathways relevant for RNA processing (FASTKD2, DDX20, IVNS1ABP, MTPAP, DICER1, POLR2L), miRNA biogenesis (DICER1, PUM1, SMAD2) and glucagon-related gluconeogenesis (EP300, PRKAB1) (Supplemental Figure 3 and Supplemental Table 3).

mIL-18+ macrophages show peculiar ultrastructural properties and mitochondrial dysfunction

We analyzed the subcellular characteristics of sorted mIL-18-positive and -negative macrophages using transmission electron microscope (TEM). Notable cytomorphological and ultrastructural distinctions between the macrophage subsets were detected. Despite the similar size and nuclear shape (with an average diameter ranging from 9.42 to 16.39 µm), a pronounced plasma membrane remodeling in mIL-18+ macrophages was observed; in particular, they were characterized by flattening of the plasma membrane with reduced numbers but increased length of cell protrusions (Figure 4A).[40]

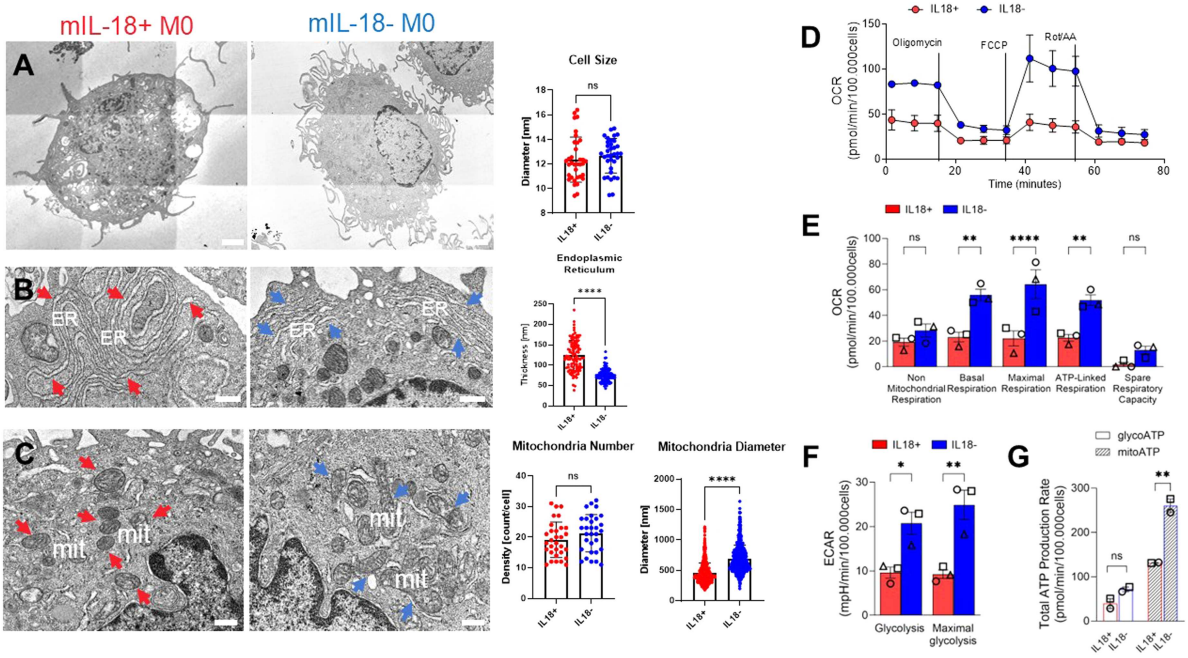

Figure 4. Transmission electron microscopy (TEM) analysis and mitochondrial metabolic activity of sorted mIL-18+ and mIL-18- macrophages. (A) Cell size: analyzed cells $n = 35$, Mann–Whitney test, scale bar: 2 mm. (B) Reticulum size: $n = 105$, *t*-test, scale bar 500 nm. (C) Mitochondria number: analyzed cells $n = 35$, *t*-test. Mitochondria diameter: analyzed mitochondria $n = 565$ for mIL-18+ and $n = 598$ for mIL-18- macrophages, Mann–Whitney test, scale bar, 500 nm. (D) Seahorse bioenergetics profile (average) OCR over time (*x*-axis) measured in mIL-18+ (gray) and mIL-18- (white) M0. Injections of Oligomycin A, FCCP, and rotenone/antimycin A (Rot/AA) are indicated with black lines. (E) Non-mitochondrial, basal, maximal, ATP-linked respiration, and spare respiratory capacity in mIL-18+ (gray columns) and mIL-18- (white columns) M0. (F) Basal and maximal ECAR after injection of Oligomycin A, in mIL-18+ (gray columns) and mIL-18- (white columns) M0. (G) Total ATP production rates in mIL-18+ and mIL-18- macrophages: Mitochondrial ATP production rate (mito ATP, white columns) and glycolytic ATP production rate (glycoATP, black columns). The graphs display the mean ± SEM of values from three independent experiments performed using macrophages derived from three healthy donors (A-F) or from two healthy donors (G). The symbols represent values from different donors. The difference between groups was analyzed by one-way ANOVA with the Bonferroni post-test by GraphPad Prism 9. ns: not significant, * = p< 0.05, ** = $p < 0.01$, *** = $p < 0{,}001$ and **** = $p < 0{,}0001$.

At the intracellular level, mIL-18+ macrophages presented numerous intracellular vacuoles (Figure 4A), a significantly enlarged endoplasmic reticulum (123.7 ± 37.2 nm in mIL-18+ versus 75.1 ± 15.6 nm in mIL-18-) (Figure 4B), and altered mitochondrial morphology (Figure 4C). Although the number of mitochondria was comparable, in mIL-18+ macrophages, they displayed a rounded shape with a significantly reduced diameter (450.5 ± 168.7 nm in mIL-18+; versus 690.3 ± 223.3 nm in mIL-18-) and were characterized by a dense matrix and less organized internal cristae.

To exclude that the engagement of mIL-18 by the mAb used for cell sorting could play a role in shaping the morphology of macrophages, TEM analysis was also performed in unstained and unsorted M0 macrophage populations. A representative analysis of a population with 64% of mIL-18+ macrophages is shown in Supplemental Figure 4. In the absence of mIL-18 engagement, macrophages showed cytomorphological and ultrastructural characteristics corresponding to what was observed in sorted mIL-18+ or mIL-18- macrophages.

TEM analysis suggested the presence of a less dynamic mitochondrial network and an energetic imbalance in mIL-18+ macrophages. To appreciate the possible functional differences in the mitochondrial compartment between mIL-18+ and mIL-18- macrophages, we evaluated mitochondrial oxidative phosphorylation and glycolytic flux and measured the oxygen consumption rate (OCR) and extracellular acidification rate (ECAR), using the Seahorse technology.

As shown in Figure 4, compared with mIL-18- macrophages, both the respiratory capacity (D and E) and aerobic glycolysis (F) of mIL-18+ macrophages were lower and not significantly altered by the metabolic modulators oligomycin (ATP-synthase inhibitor), FCCP (uncoupling agent), or rotenone/

antimycin A (inhibitors of complex I and III). Compared to mIL-18-, mIL-18+ showed a significant reduction in both basal and maximal respiration, indicative of reduced oxidative phosphorylation (OXPHOS). This finding is coupled with the oxygen consumption, which in mIL-18+ cells was less affected by ATP-synthase inhibition by oligomycin (Figure 4D). Moreover, the spare respiratory capacity, a measure of the ability of the cell to respond to increased energy demand or under stress, defined as the difference between maximal respiration and basal respiration, tends to be lower in mIL-18+ macrophages compared to the mIL-18- counterpart, although not significantly different (Figure 4E). These results were consistent with the morphologic properties of mitochondria appreciated by TEM in mIL-18+ macrophages. Notably, mIL-18+ macrophages also showed a reduction in basal glycolysis and maximal glycolytic capacity, as estimated upon oligomycin administration (Figure 4F). In agreement with these considerations, mIL-18+ cells presented a significant reduction in the total ATP production rate ($p < 0.001$) due to the low rate of ATP production associated with mitochondrial OXPHOS (Figure 4G).

These data indicate that mIL-18+ and mIL-18- macrophages are characterized by different bioenergetic profiles. In particular, mIL-18+ macrophages are in a low metabolic state with decreased mitochondrial respiration and glycolysis, while mIL-18- macrophages present an energetic metabolic phenotype associated with cell activation (high levels of OCR and ECAR).

mIL-18+ macrophages have increased endocytic properties as compared to mIL-18- macrophages

TEM analysis revealed significant differences in the plasma membrane structure between mIL-18-positive and -negative macrophages. In particular, mIL-18+ macrophages showed few and long cell protrusions associated with the emergence of large vacuolar structures (Figure 5A, Left), which resembled images of cells undergoing micropinocytosis, a non-selective clathrin-independent endocytic process driven by actin. Accordingly, the GO enrichment analysis showed the upregulation of proteins involved in vesicle

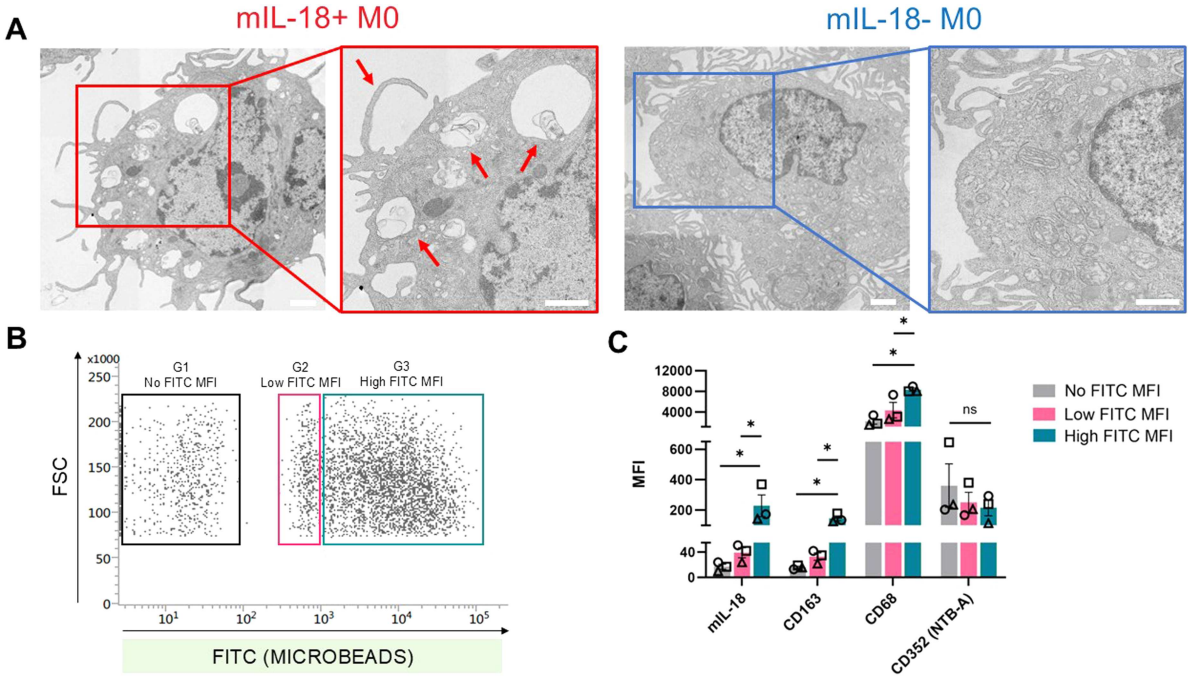

Figure 5. Endocytic properties of mIL-18+ and mIL-18- macrophages. (A) Representative TEM analysis showing the different patterns of protrusions characterizing the plasmalemma of mIL-18+ and mIL-18- M0. Scale bars: 2 µm and 500 nm. (B) Representative dot plot showing the heterogeneous fluorescent-bead uptake of M0 (null, low, or high MFI corresponding to gates 1, 2, and 3, respectively). (C) mIL-18, CD163, CD68 and CD352 (NTBA) expression in G1, G2 and G3 cells. The graphs display the mean ± SEM of values from three independent experiments performed using macrophages derived from three healthy donors. The symbols represent values from different donors. The negative controls are represented by fluorochrome-conjugated secondary or isotype-matched antibodies. The difference between groups was analyzed by one-way ANOVA with the Bonferroni post-test by GraphPad Prism 9. ns: not significant, * = $p < 0.05$.

trafficking and actin-dependent transport, including MYO5A, ITSN1, VPS36, VPS4A, and TMED (Supplemental Figure 2 and Supplemental Table 2).

To compare the endocytosis capability of mIL-18+ and mIL-18- macrophages, we performed an endocytic assay incubating unsorted M0 macrophages with carboxylate fluorescent beads. These beads mimic apoptotic bodies and efferocytosis, a critical process for clearing dying cells in both healthy and pathological tissues.[41] IF–FC analysis showed that macrophages were highly heterogeneous in terms of bead uptake, with null (Gate 1), low (Gate 2), or high (Gate 3) mean fluorescence intensities (MFI) (Figure 5B). Cells falling in the three different gates were analyzed for the expression of mIL-18 and other surface molecules. As shown in Figure 5C, macrophages characterized by high endocytosis (G3) presented significantly greater expression of mIL-18, CD163, and CD68 as compared with macrophages in the G1 and G2 regions. On the other hand, all cells, despite their endocytic capability, were characterized by comparable levels of NTB-A (CD352), a previously described macrophage-associated molecule.[28] The differences in terms of endocytosis between mIL-18+ and IL-18- macrophages were time- and dose-dependent, and a comparable endocytic capability was observed with a prolonged incubation and a greater number of beads (not shown). Supplemental Figure 5 shows representative IF–FC analysis and confocal images of beads-engulfed mIL-18+ macrophages (panels A and B, respectively).

Comparison of mIL-18 and TREM2 expression in myeloid cells present in the tumor microenvironment of adult and pediatric cancers

We previously demonstrated that CD14+ myeloid populations in the peritoneal fluid of 16 patients with ovarian cancer at different stages contained a high percentage of mIL-18+ cells with elevated surface density.[27] Here, we show that mIL-18+ cells are not limited to the peritoneal fluids of ovarian cancer patients.

We investigated the presence of mIL-18+ cells in the peritoneal fluids of adult patients with various cancer types as well as in the BM of pediatric patients affected by NB (Figure 6 and Supplemental Table 4). As shown in Figure 6A (upper panels), high percentages of mIL-18+ CD14+ cells, ranging from 70% to 98%, were identified in the peritoneal fluids of patients affected by ovarian, gastric, endometrial, colon, cervical, and pancreatic cancers. Interestingly, mIL-18+ cells expressed a wide array of surface molecules

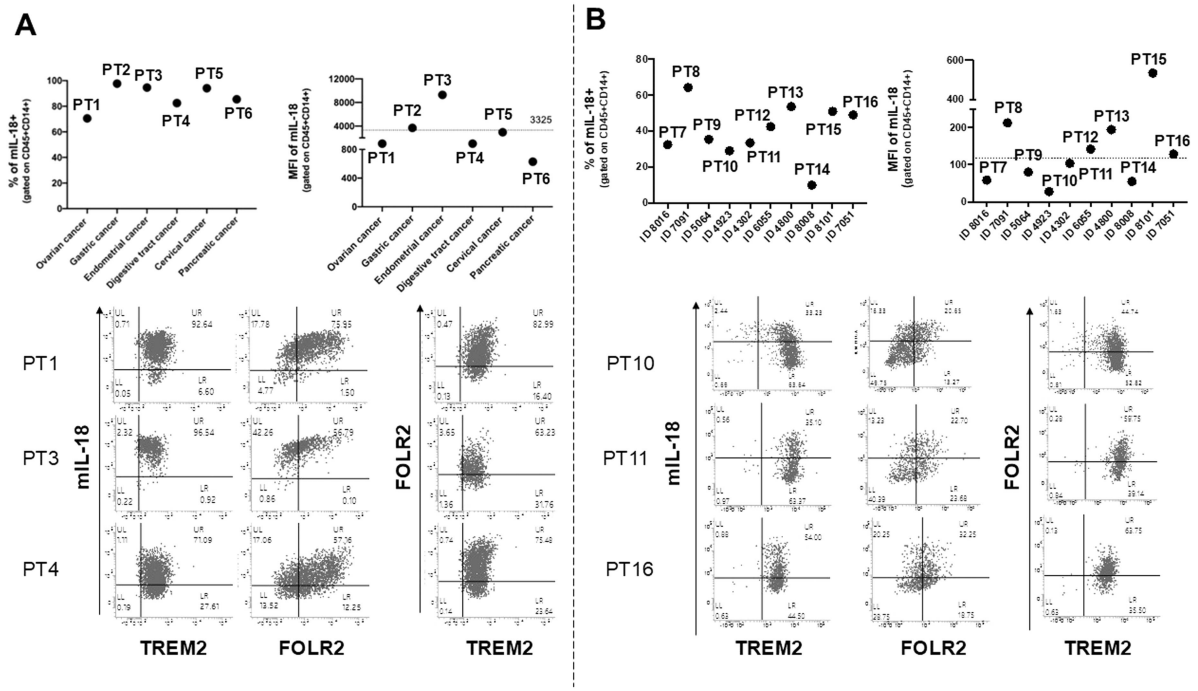

Figure 6. Detection of mIL-18+ populations in cancer specimens. CD14+ cells from the peritoneal fluids of adult cancers (A) or the BM of children with NB (B) were analyzed by IF–FC for the percentages and expression levels MFI of mIL-18 (upper panels). The lower panels show representative IF–FC analyses of mIL-18, TREM2, and FOLR2 expression.

previously detected in in vitro-derived mIL-18+ macrophages from healthy donors. These genes included CD163, CD206, CD32, CD180, CD49d, HLA-II, SIRP1α, CLEC4A, CD4, PDL1, PDL2, B7-H3, and CXCR4 (Supplemental Figure 6). Notably, the surface levels of molecules such as CLEC4, CD4, PDLs, and CXCR4 greatly varied among patients, with individuals characterized by low surface density, as in the case of PT5 affected by cervical cancer (Supplemental Figure 6B).

CD14+ myeloid cells were also compared for the expression of mIL-18, TREM2,[18] and FOLR2.[17] As shown in Figure 6A (lower panels), unlike what was observed in HDs, virtually all CD14+ cells in the peritoneal fluids were characterized by high levels of TREM2. Conversely, FOLR2 showed a more heterogeneous expression with mIL-18+ cells expressing high or low FOLR2 levels.

Relevant percentages of mIL-18+ myeloid cells, ranging from 10% to 64%, were also detectable in the BM of NB patients (Figure 6B), with or without tumor infiltration (Supplemental Table 4). Cells in BM presented lower mIL-18 expression levels (MFI 28–213, mean = 117.3) compared to those in peritoneal fluids (MFI 629-9278, mean = 3325). Similar to what was observed in peritoneal fluids, in the BM of NB patients, all the CD14+ cells expressed very high levels of TREM2, regardless of mIL-18 or FOLR2 expression. In the BM, however, a greater proportion of FOLR2+ cells lacking mIL-18 expression can be detected (Figure 6B lower panel). Representative gating strategies and negative controls are shown in Supplemental Figure 7.

Our findings provide novel insights into the relative cell surface expression of the human mIL-18, TREM2, and FOLR2 proteins. The data demonstrate an enrichment of mIL-18+ TREM2+ myeloid cells within the tumor microenvironment and reveal, based on FOLR2 expression, a previously unrecognized heterogeneity within this population.

Transcriptomic analysis of the mIL-18+ protein signature highlights gene clusters stratifying OS and EFS of NB patients

Leveraging publicly available datasets, we evaluated the prognostic significance of genes encoding the 166 proteins differentially expressed in mIL-18+ and mIL-18- macrophages. Specifically, we performed unsupervised hierarchical clustering of gene expression data from primary tumor samples collected at diagnosis from 498 NB patients. The heat map visualization revealed four distinct gene clusters: Cluster A (34 genes), Cluster B (67 genes), Cluster C (34 genes), and Cluster D (31 genes). These clusters corresponded to three patient subgroups, identified as Cluster 1 (159 patients), Cluster 2 (172 patients), and Cluster 3 (167 patients) (Figure 7A and Dataset 1).

Among the 101 upregulated genes, 34 genes from Cluster A were most highly expressed in patients from Cluster 3, while 67 genes from Cluster B were predominantly expressed in patients from Cluster 2. Among the 65 downregulated genes, 34 genes from Cluster C showed lower expression in patients from Cluster 3, and 31 genes from Cluster D were more highly expressed in this same patient cluster. These findings suggest that the expression patterns of specific gene subsets are characteristic of distinct patient groups.

Additionally, we assessed the association between patient clusters and available clinical data. Visual inspection revealed that patients in Cluster 3 were associated with poorer clinical outcomes, including older age, stage 4 disease, MYCN amplification, lower overall survival (OS) and event-free survival (EFS), an increased number of events, and a high-risk classification. Statistical analysis using the chi-square test confirmed a significant association between patient clusters and risk groups ($p < 0.001$), indicating the potential prognostic value of this gene signature.

To further evaluate the clinical relevance of the identified patient clusters, survival analysis was performed on the entire dataset (Figure 7B). The clustering significantly stratified patients in terms of OS and EFS (log-rank $p < 0.0001$), demonstrating the high prognostic value of the signature for both survival metrics. Specifically, at 5 y post-diagnosis, the OS rates for patients in Clusters 3, 2, and 1 were 50%, 80%, and >90%, respectively, while the corresponding EFS rates were 40%, 67%, and 80%, respectively.

Discussion

Macrophages are immune cells residing in virtually all healthy and pathological tissues, which originate from either embryonic/fetal precursors or circulating monocytes. Some phenotypic and functional features allow the distinction between these two different origins.[42] For example, in mouse and human brain tumors, CD49d is absent on microglia and distinguishes them from BM-derived macrophages.[25] In a

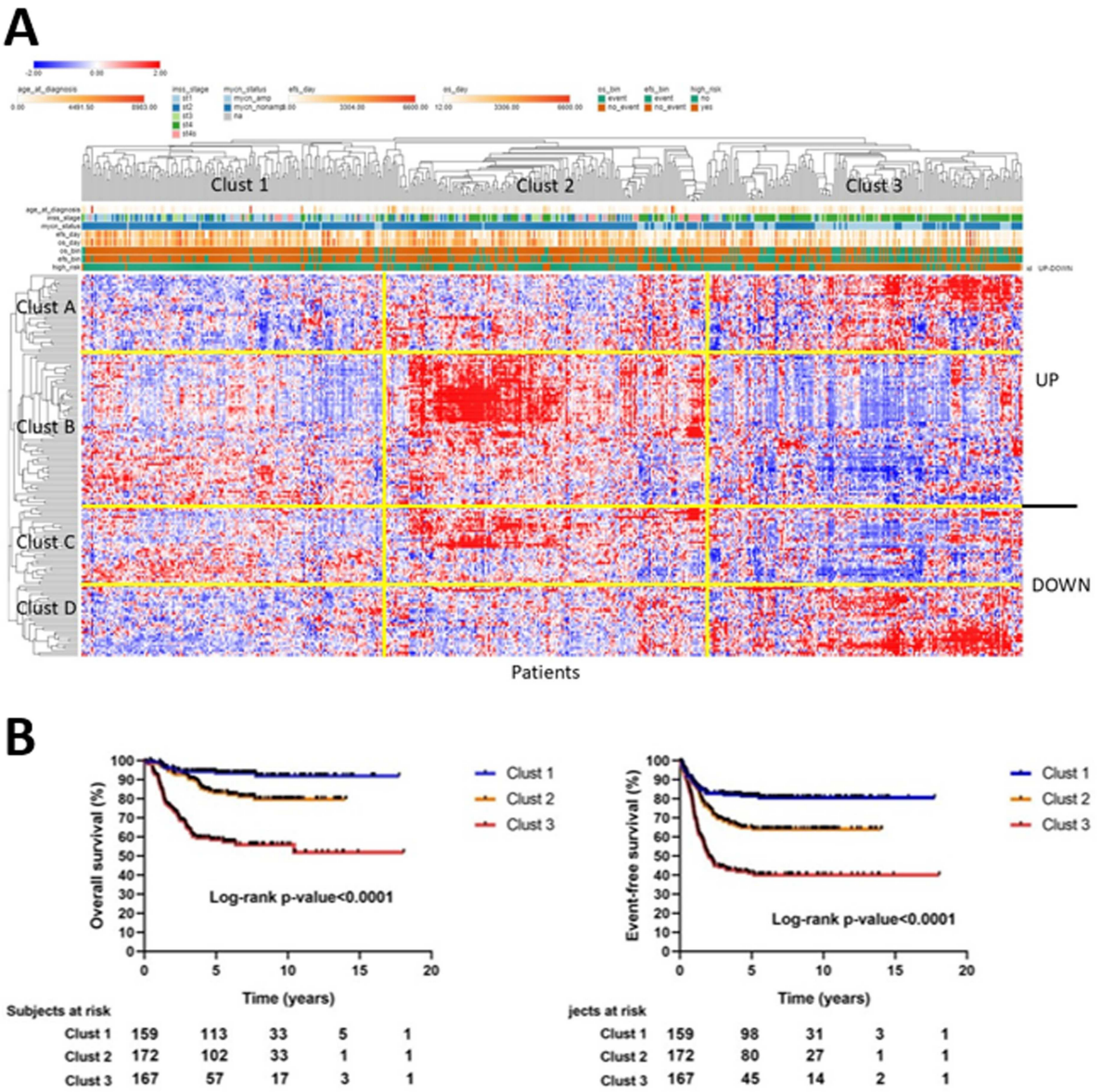

Figure 7. Heat map representation of the genes coding for the 166 proteins differentially expressed in mIL-18+ and mIL-18- macrophages. (A) Unsupervised hierarchical clustering was used to identify potential clusters. Dendrograms are shown for both rows and columns. The cluster names and yellow bars were added to the plot to improve readability. Up- or downregulated gene labels are reported on the right side. A horizontal black bar was drawn to visually differentiate up- and down-regulated genes. The expression levels were adjusted with robust z-score transformation and are indicated by a 2-color scale ranging from blue (lowest values) to red (highest values). The 2-color scale is reported in the horizontal bar at the top of the figure. Each column represents a patient, and each row represents a gene. The clinical and biological characteristics annotation of each patient was reported on top to visually evaluate the association between the clusters and unfavorable clinical features. The legend of each patient characteristic is reported on the top side of the plot. (B) Kaplan–Meier estimates of OS and EFS based on the 166-gene signature in the population of 498 NB patients. Plots are related to the OS and EFS of all patients (right and left, respectively). Survival curves for patients in cluster 1 (blue), cluster 2 (orange), and cluster 3 (red) were compared by the log-rank test, respectively. test. The log-rank *p*-value is reported at the bottom of each plot. When the log-rank *p*-value was lower than 0.0001, we indicated it as log-rank-*p*-value < 0.0001. A table reporting the number of patients at risk at each time point is shown below each plot.

murine pancreatic ductal adenocarcinoma (PDAC) model, monocyte- and embryonically derived TAMs show significant functional differences; the former has a more potent antigen presentation property, whereas the latter has a pro-fibrotic transcriptional profile, indicative of their role in tissue repair.[24] Other studies added information on the heterogeneity of macrophages in the TME, describing TREM2+ and IL-1β+ subsets with high pro-tumoral function.[18,43]

Many in vitro studies have shed light on the impact of the tissue milieu on macrophage properties. Depending on the stimuli used, unpolarized (M0) macrophages can polarize in vitro into classically activated macrophages (M1) or different types of alternatively activated macrophages (M2a, b, c, and d) that differ in their secretory profile and phenotypic traits. In vitro-derived M0, M1, and M2 macrophages are typically distinguished by the differential expression of CD80, CD86, and scavenger receptors such as CD163 and CD206. Over time, a few additional surface markers have been identified to better address macrophage heterogeneity, with mIL-18 emerging as one such marker. This study provides a detailed, multidisciplinary characterization of mIL-18+ macrophages and investigates their presence across various tumor microenvironments.

We show that TREM2 is expressed at low levels in M0 macrophages derived from HDs while showing high expression on the CD14 myeloid compartment of peritoneal fluids of adult cancer patients, and BM of NB children; in the latter, a greater heterogeneity in both mIL-18 surface density and the proportion of positive cells was observed. TREM2+ macrophages have been shown to colonize tumors, with a negative impact on prognosis, where they co-express APOE, APOC1, CD81, MERTK, STAB1, or FABP5.[18] All these proteins were detected in our proteomic analysis, but without statistically significant differences between the mIL-18+ and mIL-18- subsets. This aligns with our results showing a similar distribution in mIL-18+ and mIL-18- cells in HDs and cancer patients.

The endocytic activity, vesicular trafficking, and lipid catabolism described for mIL-18+ macrophages resemble the characteristics of the TREM2+ population described in non-small cell lung cancer by M. Merad and colleagues.[12] However, a percentage of mIL-18+ cells can also express FOLR2, identifying a subset that, unlike TREM2+ cells, may exert anti-tumoral properties.[17] Functional experiments performed using carboxylate beads, which mimic apoptotic bodies, demonstrated the high endocytic capability of mIL-18+ cells. Accordingly, the TEM analysis of mIL-18+ macrophages shows long and elaborate membrane protrusions and large vacuole structures with morphological aspects resembling micropinocytosis. Interestingly, these morphological features mirror those described for FOLR2+ macrophages by Nalio Ramos and colleagues. Although FOLR2 was not detected in the proteomic analysis, it was identified by IF-FC in in vitro-differentiated macrophages from healthy donors and in CD14+ myeloid cells from cancer patients. Thus, while all IL-18+ macrophages express TREM2 to varying degrees depending on the physiological or pathological context, they can be either FOLR2-positive or FOLR2-negative. Thus, the combined use of IF–FC of mIL-18, TREM2, and FOLR2 surface markers can define up to four distinct macrophage subsets, further underscoring the complexity of the macrophage landscape and suggesting diverse functional roles within pathological tissues.

Very recently, scRNAseq analysis identified six different TAM populations in pancreatic cancer.[43] These include an IL-1β+ population sustaining tumor-promoting inflammation; this is intriguing considering that IL−1 and IL-18 are members of the same molecular family. Our proteomic analysis shows that mIL-18+ macrophages express several proteins characterizing TAM subsets in pancreatic cancer; these molecules include IL-1β, CCL3 as well as MKI67, HSPA6, SERPINH1, HSPB, HSPD1, SPP1, FBP1, APOC1, LIPA, MRC1, MT1H, and MT1X. However, according to our proteomic dataset, IL-1β and CCL3, which are specific markers of the IL-1β+ subset, were similarly expressed in mIL-18+ and mIL-18- cells. Conversely, with both proteomic and IF–FC analysis, we detected an additional set of surface molecules differentially expressed in mIL-18+ and mIL-18- cells; these include the CD163 and CD206 scavenger receptors and molecules involved in pathogen recognition, such as CLEC4A, TLR1, FCGR2A, CD209, NRP1, and CD4. Interestingly, NRP1 favors SARS-CoV-2 infection,[44] and CD4 is the main receptor for HIV; this finding suggests that this population may play a peculiar role in the pathogenesis of these infectious diseases.

Overall, these data may indicate that mIL-18+ macrophages could be particularly active in monitoring pathological and healthy tissues through the phagocytosis of pathogens or apoptotic bodies from tumors or healthy cells. In this context, compared to mIL-18-, mIL-18+ cells have a lower expression of SIRP1α, a receptor limiting the endocytosis through the recognition of the “don’t eat me” signal CD47 on target cells or apoptotic bodies. The downregulation of SIRP1α together with the upregulation of proteins involved in endocytosis and vesicular trafficking such as MYO5A, ITSN1, VPS36, VPS4A, and TMED7 align with the abundance of vesicles observed in mIL-18+ cells, with have a morphology resembling vacuoles originating from micropinocytosis On the contrary, the proteomic analysis does not show significant differences in the

expression of lysosomal-associated molecules such as LAMP1, LAMP2, SCARB2, BLOC1S2, and BLOC1S5.

The elevated endocytosis causes the intake of large amounts of macromolecules. This may be consistent with the detection of an increased repertoire of proteins involved in the catabolic and vesicular pathways in mIL-18+ cells and, conversely, a reduction of the anabolic pathways. Our data show that mIL-18+ macrophages have a peculiar bioenergetic profile characterized by high expression of proteins involved in the catabolism of glycogen (PYGL, PYGM, RPE), triglycerides, and fatty acids (PLB2, EHHADH, ECI2, PYGM). Importantly, an increase in fatty acid oxidation as a primary energy source is described during high efferocytosis activity. This metabolic shift supports long-term energy demands during the clearance of apoptotic cells. Conversely, highly energy-demanding biosynthetic processes such as fatty acid synthesis seem to be less active and affected by the downregulation of the MCAT enzyme. Finally, protein synthesis appears to be reduced since enzymes involved in the translation and protein folding are downregulated (POLR2L, EF2B5, RPS11, and TMX1).

Overall, the decrease in the anabolic pathways governing lipid and protein synthesis and the increase in glycogen and lipidic catabolic processes may represent a compensatory mechanism to obtain energy. Accordingly, the functional assays addressing mitochondrial activity show that the mitochondrial ATP synthesis, but not the glycolysis-derived ATP, is significantly impaired in mIL-18+ cells. These observations are supported by the presence in mIL-18+ macrophages of round-shaped mitochondria with significantly reduced diameter, a dense matrix, less structured internal cristae, and the reduction of MINOS1, an enzyme involved in cristae organization. These findings suggest the presence of a less dynamic mitochondrial network and an energetic imbalance in mIL-18+ macrophages. In support of the latter observation, the transcription factor TFEB, a master regulator of autophagy[45,46] and mitochondrial quality control,[47] appears to be significantly downregulated in mIL-18+ cells. mIL-18+ macrophages also show a reduction of enzymes involved in glutathione (GCLC) and arginine synthesis (ASL).

In this scenario, mIL-18+ macrophages may represent an early subpopulation of macrophages differentiating from recruited monocytes. Similarly, "myeloid cells" from cancer patients present some phenotypic characteristics similar to those of in vitro-derived M0 macrophages, such as up-regulated CD32, CD180, CD4, and CD206 expression while retaining significant CD14 levels. These cells show properties indicative of the monitoring of the microenvironment, contributing to homeostasis maintenance, and detection of pathogens or transformed cells. Moreover, mIL-18+ cells could more efficiently migrate toward inflamed tissues; this hypothesis is in line with the high expression of molecules relevant for chemotaxis, extravasation, and migration, such as CCR2, CXCR4, CD49d,[48,49] F11R (JAMA),[50] and striatin-4.[51] The abundance of mIL-18+ CD14+ CXCR4+ CD49d+ cells, that we observed in the peritoneal inflammatory fluids of cancer patients, aligns with this phenotypic trait.

To further investigate the role of mIL-18+ cells in tumors, we analyzed publicly available gene expression profiles from primary tumors collected at diagnosis from 498 NB patients.[52] The genes coding for the proteins up- or down-regulated in mIL-18+ cells clustered into four different groups, which identified three clusters of patients with significantly different OS and EFS. This suggests that the mIL-18+ population can be further subdivided in vivo into subpopulations with different prognostic values.

The significance of mIL-18+ cells may be greater than what is discussed above. The mIL-18+ CD14+ populations can also be detected in the BM, as demonstrated by analyzing NB patients with or without BM metastases. However, the surface densities of mIL-18 are generally lower as compared to those observed in of mIL-18+ cells colonizing peritoneal fluids. It may be important to shed light on the phenotypic and functional characteristics of this peculiar BM subset; unfortunately, owing to limitations in the sample size, we were unable to deepen their characterization. Along this line, conflicting with the high expression of CD163 and CD206 scavenger receptors in mIL-18+ cells, preliminary data show that this subset is virtually absent in normal spleens obtained from cadaveric heart-beating donors; this makes their involvement in the physiological process of hemocateresis unlikely to take place.

Overall, our study further dissects macrophage heterogeneity, particularly characterizing surface marker traits. We show for the first time that mIL-18 identifies a human macrophage population with peculiar proteomic, ultrastructural, endocytic, and metabolic properties. The RNA-Seq analysis could provide valuable insights, particularly in the context of cancer patients, and may help to clarify the role of mIL-18+ cells in both physiological and pathological conditions. However, it is important to note that clustering

based only on IL-18 mRNA expression may have limited utility, as IL-18 mRNA is detectable in monocytes (mIL-18-), and macrophages, regardless of mIL-18 protein expression.[28] Additionally, reference to publicly available data could further elucidate the immunoregulatory functions of mIL-18+ cells. In this context, we already showed that mIL-18 is shed from the cell surface upon TLR stimulation with bacterial products, and sIL-18 contributes to NK cell activation.[27,28] Evaluating the role of mIL-18 macrophages in the suppressive tumor microenvironment, where synergic pro-inflammatory cytokines (i.e., IL-12 or IL-15) are scarce. Notably, depending on the cytokine milieu, IL-18 can function as either a TH1- or TH2-driving cytokine,[53] for example, by potentiating immunosuppressive factors such as TGF-β.[30]

Disclosure of potential conflicts of interest

E. Vivier is a co-founder, Senior Vice President, and Chief Scientific Officer of INNATE Pharma (Marseille, France). The other authors declare no conflict of interest.

Acknowledgments

We thank blood volunteer healthy donors, cancer patients and their families, and the University of Genova for funding the acquisition of the HITACHI 120 kV TEM microscope HT7800 (Grant D.R. 3404, 2018, Heavy Equipment).

We thank the BIT-Gaslini Biobank (IRCCS Istituto Giannina Gaslini, Genova, Italy) for providing biological specimens and Fondazione Italiana per la Lotta al Neuroblastoma for their support.

C. Vitale obtained her PhD during her participation in the study and M. Morini is currently a PhD student in Clinical and Experimental Immunology, at the School of Medical and Pharmaceutical Science, University of Genova, Italy.

F. Bellora was the recipient of a research grant awarded by AIRC from 2011 to 2018.

Author contributions

Conceptualization: C.V., K.C., A.D., D.C., F.B., S.B., F.P., M.L., G.D.N., M.C., E.V., C.B., R.C.; Data Curation: C.V., A.P., K.C., S.C., A.D., C.L., D.C., F.B., P.A., F.L., S.Bruno; Formal Analysis: C.V., A.P., S.C., A.D., C.L., D.C., F.B., P.A., S. Bruno., M.S; Funding Acquisition: M.L., G.D.N., C.B.; Investigation: C.V., K.C., S.C., A.D., C.L., D.C., F.B., P.A., S.B., F.P., S.Bruno; Methodology: C.V., K.C., A.P., S.C., C.L., D.C., F.L., S.B.; F.P., S.Bruno; Resources: M.M., F.L., A. Pessino, S.M., A.G., M.C.; Supervision R.C., C.B.; Validation: A.P., C.L., D.C. M.S; Writing – Original Draft: C.V., A.P., K.C., S.C., D.C., M.M., C.B., R.C.; Writing – Review & Editing: A.Pessino, S.M., A.G., M.C., M.L., G.D.N., M.C., E.V., C.B., R.C.

Funding

This research was funded by the Italian Ministry of Health, "5 per mille" (project 5M-2018-23680422), and Ricerca Corrente to C. B.; Italian Ministry of Health PRIN2020PBS5MJ, MUR (Ministero dell'Università e della Ricerca) to K. C.; PRIN 2022 7KTSAT, European Commission Ref EUROPEAID/173691/DD/ACT/XK to GDN, PNRR Missione 4 (Progetto CN3 – National Center for Gene Therapy and Drugs based on RNA Technology) PNRR Missione 6 (PNRR-MAD–2022–12375913) to G. D. N.; PRIN: Progetto PRIN–2022, prot. 2022J2NWKM to M. L.; Fondazione Italiana Per La Lotta Al Neuroblastoma.

ORCID

Roberta Castriconi 0000-0003-2806-1115

Data availability statement

The data obtained from the high-resolution liquid chromatography and tandem mass spectrometry (LC–MS/MS) analysis have been deposited in the ProteomeXchange Consortium via the PRIDE partner repository (dataset identifier PXD058726) and will be available upon reasonable request.

References

1. Demaria O, Cornen S, Daëron M, Morel Y, Medzhitov R, Vivier E. Harnessing innate immunity in cancer therapy. Nature. 2019;574(7776):45–56. doi: 10.1038/s41586-019-1593-5.
2. Lei Q, Wang D, Sun K, Wang L, Zhang Y. Resistance mechanisms of anti-PD1/PDL1 therapy in solid tumors. Front Cell Dev Biol. 2020;8:672. doi: 10.3389/fcell.2020.00672.
3. Zhao Z, Zheng L, Chen W, Weng W, Song J, Ji J. Delivery strategies of cancer immunotherapy: recent advances and future perspectives. J Hematol Oncol. 2019;12(1):126. doi: 10.1186/s13045-019-0817-3.
4. Kazama A, Bilim V, Tasaki M, Anraku T, Kuroki H, Shirono Y, Murata M, Hiruma K, Tomita Y. Tumor-infiltrating immune cell status predicts successful response to immune checkpoint inhibitors in renal cell carcinoma. Sci Rep. 2022;12(1):20386. doi: 10.1038/s41598-022-24437-6.
5. Zhang Y, Zhang Z. The history and advances in cancer immunotherapy: understanding the characteristics of tumor-infiltrating immune cells and their therapeutic implications. Cell Mol Immunol. 2020;17(8):807–821. doi: 10.1038/s41423-020-0488-6.
6. Vitale C, Marzagalli M, Scaglione S, Dondero A, Bottino C, Castriconi R. Tumor microenvironment and hydrogel-based 3D cancer models for in vitro testing immunotherapies. Cancers. 2022;14(4):1013. doi: 10.3390/cancers14041013.
7. Fakih M, Ouyang C, Wang C, Tu TY, Gozo MC, Cho M, Sy M, Longmate JA, Lee PP. Immune overdrive signature in colorectal tumor subset predicts poor clinical outcome. J Clin Investig. 2019;129(10):4464–4476. doi: 10.1172/JCI127046.
8. Guo S, Chen X, Guo C, Wang W. Tumour-associated macrophages heterogeneity drives resistance to clinical therapy. Expert Rev Mol Med. 2022;24:e17. doi: 10.1017/erm.2022.8.
9. Cózar B, Greppi M, Carpentier S, Narni-Mancinelli E, Chiossone L, Vivier E. Tumor-infiltrating natural killer cells. Cancer Discov. 2021;11(1):34–44. doi: 10.1158/2159-8290.CD-20-0655.
10. Mattiola I, Tomay F, De Pizzol M, Silva-Gomes R, Savino B, Gulic T, Doni A, Lonardi S, Astrid Boutet M, Nerviani A, et al. The macrophage tetraspan MS4A4A enhances dectin-1-dependent NK cell-mediated resistance to metastasis. Nat Immunol. 2019;20(8):1012–1022. doi: 10.1038/s41590-019-0417-y.
11. Vitale C, Bottino C, Castriconi R. Monocyte and macrophage in neuroblastoma: blocking their pro-tumoral functions and strengthening their crosstalk with natural killer cells. Cells. 2023;12(6):885. doi: 10.3390/cells12060885.
12. Park MD, Reyes-Torres I, LeBerichel J, Hamon P, LaMarche NM, Hegde S, Belabed M, Troncoso L, Grout JA, Magen A, et al. TREM2 macrophages drive NK cell paucity and dysfunction in lung cancer. Nat Immunol. 2023;24(5):792–801. doi: 10.1038/s41590-023-01475-4.
13. Chiossone L, Vivier E. Bringing natural killer cells to the clinic. J Exp Med. 2022;219(10):e20220830. doi: 10.1084/jem.20220830.
14. Strizova Z, Benesova I, Bartolini R, Novysedlak R, Cecrdlova E, Foley LK, Striz I. M1/M2 macrophages and their overlaps – myth or reality? Clin Sci. 2023;137(15):1067–1093. doi: 10.1042/CS20220531.
15. Locati M, Curtale G, Mantovani A. Diversity, mechanisms, and significance of macrophage plasticity. Annu Rev Pathol Mech Dis. 2020;15(1):123–147. doi: 10.1146/annurev-pathmechdis-012418-012718.
16. Wagner J, Rapsomaniki MA, Chevrier S, Anzeneder T, Langwieder C, Dykgers A, Rees M, Ramaswamy A, Muenst S, Soysal SD, et al. A single-cell atlas of the tumor and immune ecosystem of human breast cancer. Cell. 2019;177(5):1330–1345.e18. doi: 10.1016/j.cell.2019.03.005.
17. Nalio Ramos R, Missolo-Koussou Y, Gerber-Ferder Y, Bromley CP, Bugatti M, Núñez NG, Tosello Boari J, Richer W, Menger L, Denizeau J, et al. Tissue-resident FOLR2+ macrophages associate with CD8+ T cell infiltration in human breast cancer. Cell. 2022;185(7):1189–1207.e25. doi: 10.1016/j.cell.2022.02.021.
18. Molgora M, Liu YA, Colonna M, Cella M. TREM2: a new player in the tumor microenvironment. Semin Immunol. 2023;67:101739. doi: 10.1016/j.smim.2023.101739.
19. Molgora M, Esaulova E, Vermi W, Hou J, Chen Y, Luo J, Brioschi S, Bugatti M, Omodei AS, Ricci B, et al. TREM2 modulation remodels the tumor myeloid landscape enhancing anti-PD-1 immunotherapy. Cell. 2020;182(4):886–900.e17. doi: 10.1016/j.cell.2020.07.013.
20. Hoeffel G, Ginhoux F. Fetal monocytes and the origins of tissue-resident macrophages. Cell Immunol. 2018;330:5–15. doi: 10.1016/j.cellimm.2018.01.001.
21. Gordon S, Plüddemann A, Martinez Estrada F. Macrophage heterogeneity in tissues: phenotypic diversity and functions. Immunol Rev. 2014;262(1):36–55. doi: 10.1111/imr.12223.
22. Epelman S, Lavine KJ, Randolph GJ. Origin and functions of tissue macrophages. Immunity. 2014;41(1):21–35. doi: 10.1016/j.immuni.2014.06.013.
23. Ginhoux F, Guilliams M. Tissue-resident macrophage ontogeny and homeostasis. Immunity. 2016;44(3):439–449. doi: 10.1016/j.immuni.2016.02.024.
24. Zhu Y, Herndon JM, Sojka DK, Kim K-W, Knolhoff BL, Zuo C, Cullinan DR, Luo J, Bearden AR, Lavine KJ, et al. Tissue-resident macrophages in pancreatic ductal adenocarcinoma originate from embryonic hematopoiesis and promote tumor progression. Immunity. 2017;47(3):597. doi: 10.1016/j.immuni.2017.08.018.

25. Bowman RL, Klemm F, Akkari L, Pyonteck SM, Sevenich L, Quail DF, Dhara S, Simpson K, Gardner EE, Iacobuzio-Donahue CA, et al. Macrophage ontogeny underlies differences in tumor-specific education in brain malignancies. Cell Rep. 2016;17(9):2445–2459. doi: 10.1016/j.celrep.2016.10.052.
26. Lopez-Yrigoyen M, Cassetta L, Pollard JW. Macrophage targeting in cancer. Ann NY Acad Sci. 2021;1499(1):18–41. doi: 10.1111/nyas.14377.
27. Bellora F, Castriconi R, Dondero A, Pessino A, Nencioni A, Liggieri G, Moretta L, Mantovani A, Moretta A, Bottino C. TLR activation of tumor-associated macrophages from ovarian cancer patients triggers cytolytic activity of NK cells. Eur J Immunol. 2014;44(6):1814–1822. doi: 10.1002/eji.201344130.
28. Bellora F, Castriconi R, Doni A, Cantoni C, Moretta L, Mantovani A, Moretta A, Bottino C. M-CSF induces the expression of a membrane-bound form of IL -18 in a subset of human monocytes differentiating in vitro toward macrophages. Eur J Immunol. 2012;42(6):1618–1626. doi: 10.1002/eji.201142173.
29. Bellora F, Castriconi R, Dondero A, Reggiardo G, Moretta L, Mantovani A, Moretta A, Bottino C. The interaction of human natural killer cells with either unpolarized or polarized macrophages results in different functional outcomes. Proc Natl Acad Sci USA. 2010;107(50):21659–21664. doi: 10.1073/pnas.1007654108.
30. Casu B, Dondero A, Regis S, Caliendo F, Petretto A, Bartolucci M, Bellora F, Bottino C, Castriconi R. Novel immunoregulatory functions of IL-18, an accomplice of TGF-β1. Cancers. 2019;11(1):75. doi: 10.3390/cancers11010075.
31. Tyanova S, Temu T, Cox J. The MaxQuant computational platform for mass spectrometry-based shotgun proteomics. Nat Protoc. 2016;11(12):2301–2319. doi: 10.1038/nprot.2016.136.
32. Tyanova S, Temu T, Sinitcyn P, Carlson A, Hein MY, Geiger T, Mann M, Cox J. The Perseus computational platform for comprehensive analysis of (prote)omics data. Nat Methods. 2016;13(9):731–740. doi: 10.1038/nmeth.3901.
33. Ge SX, Jung D, Yao R. ShinyGO: a graphical gene-set enrichment tool for animals and plants Valencia A, editor. Bioinformatics. 2020;36(8):2628–2629. doi: 10.1093/bioinformatics/btz931.
34. Evangelista JE, Xie Z, Marino GB, Nguyen N, Clarke DJB, Ma'ayan A. Enrichr-KG: bridging enrichment analysis across multiple libraries. Nucleic Acids Res. 2023;51(W1):W168–W179. doi: 10.1093/nar/gkad393.
35. Dondero A, Morini M, Cangelosi D, Mazzocco K, Serra M, Spaggiari GM, Rotta G, Tondo A, Locatelli F, Castellano A, et al. Multiparametric flow cytometry highlights B7-H3 as a novel diagnostic/therapeutic target in GD2neg/low neuroblastoma variants. J Immunother Cancer. 2021;9(4):e002293. doi: 10.1136/jitc-2020-002293.
36. Marzagalli M, Pelizzoni G, Fedi A, Vitale C, Fontana F, Bruno S, Poggi A, Dondero A, Aiello M, Castriconi R, et al. A multi-organ-on-chip to recapitulate the infiltration and the cytotoxic activity of circulating NK cells in 3D matrix-based tumor model. Front. Bioeng. Biotechnol. 2022;10:945149. doi: 10.3389/fbioe.2022.945149.
37. Swerts K, Ambros PF, Brouzes C, Navarro JMF, Gross N, Rampling D, Schumacher-Kuckelkorn R, Sementa AR, Ladenstein R, Beiske K. Standardization of the immunocytochemical detection of neuroblastoma cells in bone marrow. J Histochem Cytochem. 2005;53(12):1433–1440. doi: 10.1369/jhc.5C6661.2005.
38. Cohn SL, Pearson ADJ, London WB, Monclair T, Ambros PF, Brodeur GM, Faldum A, Hero B, Iehara T, Machin D, et al. The international neuroblastoma risk group (INRG) classification system: an INRG Task Force Report. JCO. 2009;27(2):289–297. doi: 10.1200/JCO.2008.16.6785.
39. Stolfi C, Troncone E, Marafini I, Monteleone G. Role of TGF-beta and Smad7 in gut inflammation, fibrosis and cancer. Biomolecules. 2020;11(1):17. doi: 10.3390/biom11010017.
40. Mylvaganam S, Freeman SA, Grinstein S. The cytoskeleton in phagocytosis and macropinocytosis. Curr Biol. 2021;31(10):R619–R632. doi: 10.1016/j.cub.2021.01.036.
41. Martin CJ, Peters KN, Behar SM. Macrophages clean up: efferocytosis and microbial control. Curr Opin Microbiol. 2014;17:17–23. doi: 10.1016/j.mib.2013.10.007.
42. Ginhoux F, Schultze JL, Murray PJ, Ochando J, Biswas SK. New insights into the multidimensional concept of macrophage ontogeny, activation and function. Nat Immunol. 2016;17(1):34–40. doi: 10.1038/ni.3324.
43. Caronni N, La Terza F, Vittoria FM, Barbiera G, Mezzanzanica L, Cuzzola V, Barresi S, Pellegatta M, Canevazzi P, Dunsmore G, et al. IL-1β+ macrophages fuel pathogenic inflammation in pancreatic cancer. Nature. 2023;623(7986):415–422. doi: 10.1038/s41586-023-06685-2.
44. Cantuti-Castelvetri L, Ojha R, Pedro LD, Djannatian M, Franz J, Kuivanen S, Van Der Meer F, Kallio K, Kaya T, Anastasina M, et al. Neuropilin-1 facilitates SARS-CoV-2 cell entry and infectivity. Science. 2020;370(6518):856–860. doi: 10.1126/science.abd2985.
45. Li Y, Hodge J, Liu Q, Wang J, Wang Y, Evans TD, Altomare D, Yao Y, Murphy EA, Razani B, et al. TFEB is a master regulator of tumor-associated macrophages in breast cancer. J Immunother Cancer. 2020;8(1):e000543. doi: 10.1136/jitc-2020-000543.
46. Bellese G, Tagliatti E, Gagliani MC, Santamaria S, Arnaldi P, Falletta P, Rusmini P, Matteoli M, Castagnola P, Cortese K. Neratinib is a TFEB and TFE3 activator that potentiates autophagy and unbalances energy metabolism in ERBB2+ breast cancer cells. Biochem Pharmacol. 2023;213:115633. doi: 10.1016/j.bcp.2023.115633.
47. Wang S, Chen Y, Li X, Zhang W, Liu Z, Wu M, Pan Q, Liu H. Emerging role of transcription factor EB in mitochondrial quality control. Biomed Pharmacother. 2020;128:110272. doi: 10.1016/j.biopha.2020.110272.

48. Dal Bo M, Tissino E, Benedetti D, Caldana C, Bomben R, Del Poeta G, Gaidano G, Rossi FM, Zucchetto A, Gattei V. Microenvironmental interactions in chronic lymphocytic leukemia: the master role of CD49d. Semin Hematol. 2014;51(3):168–176. doi: 10.1053/j.seminhematol.2014.05.002.
49. Pasikowska M, Walsby E, Apollonio B, Cuthill K, Phillips E, Coulter E, Longhi MS, Ma Y, Yallop D, Barber LD, et al. Phenotype and immune function of lymph node and peripheral blood CLL cells are linked to transendothelial migration. Blood. 2016;128(4):563–573. doi: 10.1182/blood-2016-01-683128.
50. Koehler M, Aravamudhan P, Guzman-Cardozo C, Dumitru AC, Yang J, Gargiulo S, Soumillion P, Dermody TS, Alsteens D. Glycan-mediated enhancement of reovirus receptor binding. Nat Commun. 2019;10(1):4460. doi: 10.1038/s41467-019-12411-2.
51. Wang Z, Li Y, Cao J, Zhang W, Wang Q, Zhang Z, Gao Z, Ye Y, Jiang K, Wang S. MicroRNA profile identifies miR-6165 could suppress gastric cancer migration and invasion by targeting STRN4. OTT. 2020;Volume 13:1859–1869. doi: 10.2147/OTT.S208024.
52. Zhang W, Yu Y, Hertwig F, Thierry-Mieg J, Zhang W, Thierry-Mieg D, Wang J, Furlanello C, Devanarayan V, Cheng J, et al. Comparison of RNA-seq and microarray-based models for clinical endpoint prediction. Genome Biol. 2015;16(1):133. doi: 10.1186/s13059-015-0694-1.
53. Novick D, Kim S, Kaplanski G, Dinarello CA. Interleukin-18, more than a Th1 cytokine. Semin Immunol. 2013;25(6):439–448. doi: 10.1016/j.smim.2013.10.014.